

doi: 10.15407/ujpe61.10.0863

A.V. UKLEIN,<sup>1</sup> V.E. DIYUK,<sup>2</sup> L.M. GRISHCHENKO,<sup>2</sup> V.O. KOZHANOV,<sup>2</sup>  
V.V. LISNYAK,<sup>2</sup> V.V. MULTIAN,<sup>1</sup> P.I. BUDNYK,<sup>1</sup> V.YA. GAYVORONSKY<sup>1</sup><sup>1</sup>Institute of Physics, Nat. Acad. of Sci. of Ukraine  
(46, Prosp. Nauky, Kyiv 03680, Ukraine; e-mail: vlad@iop.kiev.ua)<sup>2</sup>Taras Shevchenko National University of Kyiv  
(64, Volodymyrs'ka Str., Kyiv 01601, Ukraine)PACS 81.70.Pg, 65.60.+a,  
81.05.U-, 82.80.Yc,  
78.20.-e, 42.65.-k,  
42.65.An**CORRELATION OF THE PHOTOINDUCED TOTAL  
TRANSMISSION WITH THE DEGREE OF SURFACE  
FUNCTIONALIZATION OF CARBON MATERIALS  
OBTAINED FROM NATURAL RENEWABLE SOURCES**

---

For the first time, a contactless express method, which is based on the self-action of picosecond range laser pulses at 1064 nm, is used for the characterization of an optically dense porous layer of carbon material (CM) bulk particles obtained from a lignocellulosic source. It is found that the oxidation treatment reduces the Brunauer–Emmett–Teller ( $S_{\text{BET}}$ ) surface area from  $9.52 \times 10^5 \text{ m}^2/\text{kg}$  to  $2.73 \times 10^5 \text{ m}^2/\text{kg}$ . This reduction occurs due to the destruction of the carbon matrix fraction and to the formation of novel O-containing surface groups. The concentrated 30-mass%  $\text{HNO}_3$  is found to be the most efficient oxidant giving the highest yield of carboxylic (Cb), anhydridic, lactonic, and phenolic surface functionalities. The concentration of the surface functional groups is determined in a dynamic argon atmosphere by thermogravimetric (TG) analysis and thermoprogrammed desorption coupled with IR (TPD-IR) spectroscopy. The surface acidity defined from data of the Boehm titration shows the acceptable agreement with the data of TG-TPD-IR examination. An enhancement of the surface hydrophilicity allows the use of carbon matrix for the covalent binding of bioligands, amino acids, their residues, and proteins to the oxygen-containing functionalities, such as Cb groups. The observed photoinduced absorption efficiency of the bulk carbon particles  $\text{Im}(\chi_{\text{C}}^{(3)}) \sim 10^{-16} \text{ m}^2/\text{W}$  is in the range of that of nanosized carbons. A slight variation of the ratio  $\text{Im}(\chi_{\text{C}}^{(3)})/S_{\text{BET}}$  within the limits of experimental errors indicates a certain correlation between the absorptive NLO response and the CM specific surface. We suggest to utilize  $\text{Im}(\chi_{\text{C}}^{(3)})$  as a quality parameter for carbon materials subjected to the oxidation, which is a typical initial step of the most commonly used functionalization routes for the preparation of biomedical materials.

*Keywords:* carbons, surface acidity, oxidation, nonlinear optical response

**1. Introduction**

The spirit of the era of integrated biomaterials synergistically links key scientific disciplines, e.g. physics,

materials chemistry, nanotechnology, and medical engineering. Biomedical nanotechnology opens a new field of applying carbons and related materials in healthcare [1, 2], since the majority of these materials show enough resistivity to protect against thermal, chemical, and biological damages [3–5]. So, in this vein, representatives of the diverse carbon fam-

---

© A.V. UKLEIN, V.E. DIYUK, L.M. GRISHCHENKO,  
V.O. KOZHANOV, V.V. LISNYAK, V.V. MULTIAN,  
P.I. BUDNYK, V.YA. GAYVORONSKY, 2016

ily have great potential to get a wide adaptation in integrated biomaterials [6–8].

Currently, a certain class of carbon materials (CMs), which are based on particles with a size typically ranging from tenths of nanometers up to micrometers, got the use in modern prosthetics. To take an example, nano-sized carbon fibers [9, 10] enter the composition of some improved neural and orthopedic implants [11–14].

But in order to adapt diverse CMs in advanced biomedical materials, it is necessary to optimize their characteristics such as the wear resistance, adhesion-wettability, and biocompatibility. In this regard, various adhesion-related characteristics of CMs attract the attention of scientists and engineers. Considering all the new achievements of applied surface science, the chemical functionalization is a universal way for improving CMs' characteristics by the regulation of surface-interface properties [9]. Among the simplest functionalization routes, the main attention should be paid to the oxidation, which is used more frequently for the preparation of medical carbons. In this regard, the preparation of new CMs with developed surface chemistry, e.g., from natural renewable resources, is of interest, as they can mimic the required surface reactivity of the known medical carbons, which are components of the best implants and related biomaterials [2, 4, 15]. However, such biocompatible materials for medical applications should take a screening of surface properties. In this case, one can find that the surface metrology is of a paramount importance in order to categorize and to adapt the medical carbons.

Recently, the nonlinear optical (NLO) properties of nanoscale carbons of the various types and dimensions were reported in [16–18]. Carbon nanoparticles (NP) exhibit high nonlinear optical (NLO) responses due to the self-action of laser pulses with variable pulse duration from the ps to ns range. Such CM NPs are sufficient to be used in the optical limiting, data storage, and solar cell devices. It was shown in [16, 19] that the changes of the NLO response for various graphene derivatives allow one to execute the metrological characterization of a quality for carbon media.

From this viewpoint, the sensitive measurement of an NLO response, in particular with a single-beam laser technique, becomes a relevant approach to the comparative assessment and can be used for monitor-

ing the surface chemistry with self-action effects of ps laser pulses in medical carbons.

The main idea of the studies represented here is based on the high sensitivity of the method to the concentration of defects and to a nonstoichiometry in solids [20]. Following this paradigm, we report the NLO response, surface characteristics, and defects for some oxidized CMs of natural origin.

## 2. Experimental

Lignocellulosic material from a natural renewable source was used to obtain a carbon material (CM) by the physical activation with steam, as reported in [21]. The obtained CM was subjected to the oxidation with nitric acid ( $\text{HNO}_3$ ).

The CM grains 2 g in mass and 0.5–1 mm in size were refluxed with 60 ml of 5, 10, and 30 mass%  $\text{HNO}_3$  solutions in a sand bath for 2 h. The oxidized CM was decanted, washed with distilled water, and air-dried at 120 °C. These samples are assigned below as CM – initial sample; CM05, CM10, and CM30 are CM samples oxidized with 5, 10, and 30 mass%  $\text{HNO}_3$ , correspondingly. The Brunauer–Emmett–Teller surface area  $S_{\text{BET}}$  was measured from  $\text{N}_2$  gas adsorption with a Kelvin 1042 (Costech Microanalytical) sorptometer, the total open pore volume  $V_S$  was determined from the adsorption isotherm, and the bulk density  $\gamma$  was found, by measuring the weight of CM in a given volume. The refractive index  $n$  was measured indirectly, basing on the reflectivity of incident light measured in air and cedar oil [22].

The gravimetric porosity  $p$  was estimated from the adsorption and pycnometric data. The total oxygen was analyzed with an Oxford Inca 350 EDX spectrometer. The concentration of the surface oxygen-containing groups ( $C_B$ ) was measured by the Boehm titration [23,24]. The concentration ( $C_{\text{TPD}}$ ) and thermal stability of oxygen-containing surface groups were determined by the thermogravimetry-thermoprogrammed desorption method with IR registration of desorbed products (TG-TPD-IR), as reported in [25, 26]. In a typical experiment, the carbon sample (0.1 g) was heated from 20 to 900 °C in a flow of Ar of 50 ml/min. The heating rate was equal to 10 °C/min. The inconsistency ( $I_c$ ) criterion is defined as a ratio of sums of the concentration of carboxylic (Cb), anhydridic-lactonic (A-L), and phenolic (Ph) groups, which were obtained from the Boehm titration and TPD-IR data,  $\sum C_B / \sum C_{\text{TPD}}$ .

The measurements of the absorptive NLO response of carbon media due to the self-action of picosecond laser pulses (42 ps FWHM) at 1064 nm with a repetition rate of 15 Hz were performed according to the technique described in [27]. For the measurements, the CM powder was placed between two glass plates, which were separated with a 340  $\mu\text{m}$  thin spacer used to control the CM porous layer thickness ( $d$ ). The sample was positioned directly at the  $\varnothing$  1 cm aperture of a photodetector to avoid the scattering impact extinction. The studied samples of CM porous layers were positioned at 0.18 m after the focusing lens with a focal length of 11 cm, which provides the total transmittance variation  $T(I)$  versus the laser peak intensity  $I$  in the range from 2 to 600  $\text{MW}/\text{cm}^2$ . Each of the experimental  $T(I)$  sets was obtained due to the data acquisition of about 5000 laser shots, which resulted in a relative error of about  $\pm 0.2\%$  of the approximated curves. We have thoroughly checked up the reversibility of the obtained photodarkening effect. At  $I < 2 \text{ MW}/\text{cm}^2$ , the total transmittance  $T_0$  of the CM layers is constant, which corresponds to a linear regime of the optical response. We estimated the effective cubic NLO susceptibility  $\text{Im}(\chi_{\text{eff}}^{(3)})$  of the CM porous layer, which characterizes the efficiency of the photoinduced absorption coefficient as  $\Delta\alpha_{\text{eff}} = \alpha_{\text{eff}}(I) - \alpha_{\text{eff}} = \beta_{\text{eff}}I \sim \text{Im}(\chi_{\text{eff}}^{(3)})I$ .

Considering the spatial and temporal averagings of a transmitted pulse [27],  $T(I)$  is expressed as

$$T(I_0) = T_0 \frac{\ln(1 + \Delta\alpha_{\text{eff}}L_{\text{eff}})}{\Delta\alpha_{\text{eff}}L_{\text{eff}}} \left[ \frac{1 + 0.228\Delta\alpha_{\text{eff}}L_{\text{eff}}}{1 + 0.136\Delta\alpha_{\text{eff}}L_{\text{eff}}} \right], \quad (1)$$

where  $L_{\text{eff}} = (1 + \exp(-\alpha_{\text{eff}}d))/\alpha_{\text{eff}}$  is the effective self-action length [28].

The effective dielectric permittivity of the porous carbon layer ( $\varepsilon_{\text{eff}}$ ) one could consider as a combination of contributions of the bulk fraction ( $\varepsilon_{\text{C}}$ ) and voids ( $\varepsilon_{\text{v}} = 1$ ). Within the Looyenga formulation of the effective media approximation (EMA) approach [29, 30], we get

$$\sqrt[3]{\varepsilon_{\text{eff}}} = (1 - p)\sqrt[3]{\varepsilon_{\text{C}}} + p, \quad (2)$$

where  $p$  is the porosity. This formulation remains valid and useful for a thin layer of microporous carbons with very high porosity (about 70%). The bulk initial CM has  $n_{\text{C}}$  of about 2.0 [31]. Accounting for

the reference data for the bulk, we have also estimated the refractive index ( $n_{\text{eff}}$ ) of the porous layer as

$$n_{\text{eff}} = \left[ (1 - p)n_{\text{C}}^{2/3} + p \right]^{3/2}. \quad (3)$$

From  $n_{\text{eff}}$ , it is possible to derive the layer transmittance ( $T_{\text{eff}}$ ) and the effective absorption coefficient of the CM porous layer  $\alpha_{\text{eff}}$  as

$$T_{\text{eff}} = T_0 / \left[ (1 - R_1)(1 - R_2) \right]^2, \quad \alpha_{\text{eff}} = -(\ln T_{\text{eff}})/d. \quad (4)$$

The experimentally obtained  $T_0$  was corrected to the reflection losses provided by the air-glass ( $R_1$ ) and the glass-carbon ( $R_2$ ) interfaces

$$R_1 = \left[ (n_g - 1)/(n_g + 1) \right]^2, \quad (5)$$

$$R_2 = \left[ (n_{\text{eff}} - n_g)/(n_{\text{eff}} + n_g) \right]^2.$$

The resulting optical absorption of the bulk carbon fraction  $\alpha_{\text{C}}(I)$  can be estimated from a superposition of the linear ( $\alpha_{\text{C}}$ ) and photoinduced ( $\beta_{\text{C}}I$ ) absorptions:

$$\alpha_{\text{C}}(I) = \alpha_{\text{C}} + \beta_{\text{C}}I. \quad (6)$$

Looyenga's formulation [29] yields

$$\alpha_{\text{C}} = \alpha_{\text{eff}} \sqrt[3]{n_{\text{C}}/n_{\text{eff}}}/(1 - p), \quad (7)$$

$$\beta_{\text{C}} = \beta_{\text{eff}} \sqrt[3]{n_{\text{C}}/n_{\text{eff}}}/(1 - p),$$

where the coefficients are proportional to those of the porous layer.

### 3. Results and Discussion

The data obtained by TG-TPD-IR could be interpreted as follows: since even the thermodesorption of the gases from carbons occurs in the inert gas, the difference between the total  $\Delta m$  and the physisorbed  $\text{H}_2\text{O}$  mass loss refers to the mass of functional groups  $\Delta m_{\text{fg}}$ . Because  $\Delta m_{\text{fg}}$  sums the contributions from different groups, their separation and assignment were performed from the measurements of the concentrations of carbon oxides,  $C(\text{CO})$  and  $C(\text{CO}_2)$ . The IR intensities of released CO and  $\text{CO}_2$  were registered as functions of the time and the temperature by means of TPD-IR. The intensities referred to  $C(\text{CO})$  and  $C(\text{CO}_2)$  in Ar-diluted outlet gases were measured with accuracies of 2.0 and

**Table 1.** Texture and surface characteristics of CMs.  $S_{\text{BET}}$  – Brunauer–Emmett–Teller surface area,  $\gamma$  – bulk density,  $V_{\text{S}}$  – total open pore volume,  $O$  – total atomic % for oxygen determined by EDX analysis,  $C_{\text{fg}}$  – concentration of functional groups: carboxylic (Cb), anhydridic (A), lactonic (L), phenolic (Ph), and quinolic (Q) ones.  $C_{\text{TPD}}$  and  $C_{\text{B}}$  – concentrations of the surface oxygen-containing groups determined by thermoprogrammed desorption coupled with IR spectroscopy and Boehm titration, correspondingly.  $I_c$  – inconsistency criterion. CM – initial sample, CM05, CM10, and CM30 – CM samples oxidized with 5, 10, and 30 mass%  $\text{HNO}_3$

Sample	$S_{\text{BET}}$ $\times 10^3$ $\text{m}^2/\text{g}$	$\gamma$ $\times 10^9$ $\text{kg}/\text{m}^3$	$V_{\text{S}}$ $\times 10^{-9}$ $\text{m}^3/\text{kg}$	O, at%	Concentration ( $C_{\text{fg}}$ ), mmol/g							$I_c$ criterion
					Cb		A-L		Ph		Q	
					$C_{\text{TPD}}$	$C_{\text{B}}$	$C_{\text{TPD}}$	$C_{\text{B}}$	$C_{\text{TPD}}$	$C_{\text{B}}$	$C_{\text{TPD}}$	
CM	952	0.44	0.508	2.1	0.10	0.10	0	0	0.41	0.20	0.42	0.32
CM05	618	0.48	0.459	7.1	0.61	0.77	1.31	0.20	0.92	0.39	0	0.48
CM10	455	0.53	0.306	14.9	1.23	1.52	2.03	0.66	2.67	1.04	0	0.54
CM30	273	0.58	0.169	18.3	1.44	1.85	3.98	0.79	3.11	1.32	0	0.46

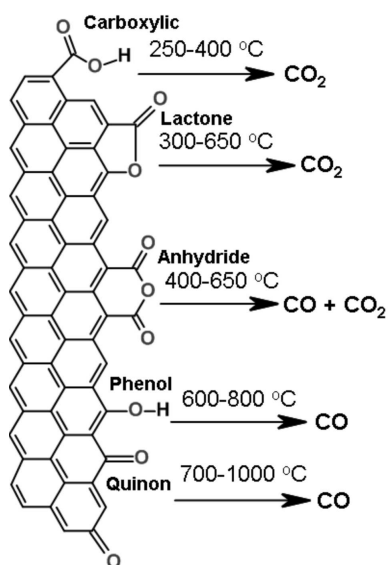


**Fig. 1.** Thermal destruction of oxygen-containing carbon surface groups, as in Refs. [32, 33]

$6.0 \times 10^{-6}$  mol/l, correspondingly. The temperature profiles recalculated onto the gas release rates  $r(\text{CO})$  and  $r(\text{CO}_2)$  were deconvoluted into the multiple components corresponding to the decomposition of certain oxygen-containing groups. The groups were separated and assigned by the temperature maxima and the range of thermodesorption (TD) of CO and  $\text{CO}_2$ , to reliably detected oxygen-containing surface groups (see Fig. 1), as Cb, A, L, Ph, and quinolic (Q) ones [32, 33]. Each of the present group concentrations  $C_{\text{fg}}$

was evaluated from the peak area analysis and listed in Table 1.

As one can see from Table 1, the oxidation with  $\text{HNO}_3$  changes the surface chemistry of CMs and textural properties. In contrast to the initial CM,  $S_{\text{BET}}$  of the oxidized CMs is reduced by 35% and up to almost  $\sim 3.5$  times, depending on the concentration of  $\text{HNO}_3$  ( $w(\text{HNO}_3)$ ). The value of  $V_{\text{S}}$  shows the same dependence and decreases with an increase of  $w(\text{HNO}_3)$  from 1.1 to 3 times. This means that the carbon matrix porous structure is destructed partially. Nm-sized particles of the oxidized carbon are leached in the form of humic acids from the carbon bulk. EDX proves an increase of the content of oxygen in the obtained CMs. Figures 2, *a* and 2, *b* demonstrate the typical TG-TPD-IR profiles for the initial and oxidized CMs. The profiles combine the mass loss in the integral (TG) and differential (DTG) forms and  $r(\text{CO}_2)/r(\text{CO})$  temperature curves.

By comparing Figs. 2, *a* and 2, *b*, it is clear that the CMs surface oxidation causes a significant mass loss registered on TG/DTG curves. In contrast to the initial CM,  $\text{CO}_2$  and CO that are realized as TD products of the oxidized CMs are  $\sim 12$ –34 and  $\sim 2$ –6 times more, correspondingly (Fig. 2, *b*, Table 1). This substantial increase of the CO/ $\text{CO}_2$  release indicates the formation of a significant amount of Cb, A–L, and Ph functional groups. Here, we analyze the temperature trend of TG-TPD-IR profiles at above 150 °C, accounting for the effect of physisorbed CO,  $\text{CO}_2$ , and  $\text{H}_2\text{O}$ . Weakly bound Cb

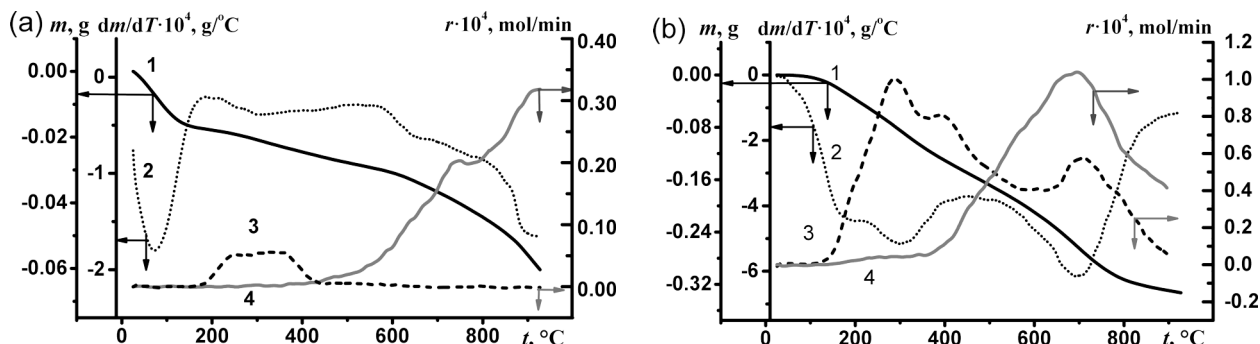


Fig. 2. Typical TG-TPD-IR profiles for initial CM (a) and CM30 (b): TG 1, DTG 2,  $r(\text{CO}_2)$  3, and  $r(\text{CO})$  4

groups, strongly-bonded A–L, Ph and/or Q groups are desorbed at the temperature intervals 180–380  $^{\circ}\text{C}$ , 380–600  $^{\circ}\text{C}$ , 600–950  $^{\circ}\text{C}$ , and/or  $>750$   $^{\circ}\text{C}$ , correspondingly. The concentrations of Cb, A–L, and Ph that obtained from the Boehm titration and TPD-IR are in a qualitative consistency (see Table 1). The titration gives higher values for Cb, than the thermal desorption, cf.  $I_c$  criterion values in Table 1. This discrepancy is concerned, in our point of a view, with two main factors as the hindering of TD of gases and the high surface-chemical reactivity of these groups, when heated. Indeed, at the heating up to 300  $^{\circ}\text{C}$ , two neighboring Cb groups can be dehydrated, by forming an A group. The latter is confirmed by a significant release of water in this temperature interval, see Fig. 2, a, b. The probability of the interaction between Cb groups obviously increases at any diffusion complications during the  $\text{CO}_2/\text{CO}$  desorption. These complications are supported by the microporous structure and by an increase of the concentration of Cb groups. The latter is achieved from the use of the more concentrated  $\text{HNO}_3$  oxidant, see Table 1. In contrast to Cb groups, the probability of the interaction between other oxygen-containing groups, as A–L and Ph, is smaller to a great extent.

As can be seen from the data in Table 1, the initial CM has diverse microporous structure. The surface layer of CM contains a small amount of oxygen-containing groups that are decomposed at high temperatures. The deep oxidation reduces the values of  $S_{\text{BET}}$  and the total open pore volume ( $V_S$ ) similarly as  $\Delta S_{\text{BET}}/S_{\text{BET}}(\text{CM}) \sim \Delta V_S/V_S(\text{CM})$ . The destruction of the porous structure essentially depends on the concentration of  $\text{HNO}_3$ . The oxidative treatment gives oxygen-containing groups, e.g., Cb and A–L ones, which are decomposed at low tempera-

tures. These groups are practically absent in the initial CM. The concentration of  $\text{HNO}_3$  does not significantly affect the ratio of different types of groups in CM05, CM10, and CM30. The surface layer of the mentioned CMs has up to 21% of Cb and the close values of A–L and Ph groups (32–46%).

Summarizing our findings, the oxidation of the CM surface with  $\text{HNO}_3$  causes the texture destruction. TG-TPD-IR can characterize indirectly the structure of surface functionalities. The temperature range of  $\text{CO}_2/\text{CO}$  release indicates the formation of Cb, A–L, and Ph groups during the oxidation. No selective functionalization with a Q groups was found that evidences the moderate oxidation regime contrasting with that of [34]. The concentrated  $\text{HNO}_3$  oxidizes efficiently the surface and gives a significant amount of oxygen-containing groups of all mentioned types. So, despite the chemical inertness of carbons, their overall chemical reactivity can be changed by

Table 2. The optical parameters of the porous carbon medium and fraction of carbon particles:  $p$  – porosity,  $n_{\text{eff}}$  – effective refractive index (Eq. (3)) of the CM porous layer,  $T_0$  – transmittance in a linear regime,  $T_{\text{eff}}$  – the corrected transmittance without impact of the reflections at interfaces,  $\alpha_{\text{eff}}$  – effective light absorption coefficient of the layer (Eq. (4)),  $\alpha_C$  – estimated light absorption coefficient of the CM fraction (Eq. (7))

Sample	$p$ , %	$n_{\text{eff}}$	$T_0$ , %	$T_{\text{eff}}$ , %	$\alpha_{\text{eff}}$ , $\times 10^2 \text{ m}^{-1}$	$\alpha_C$ , $\times 10^2 \text{ m}^{-1}$	$\alpha_C(S_{\text{BET}})^{-1}$ , $\times 10^{-2} \text{ kg/m}^3$
CM	78	1.20	1.9	2.1	113.3	610.8	6.4
CM05	76	1.23	3.6	4.0	94.7	464.0	7.5
CM10	74	1.25	3.7	4.1	94.0	422.8	9.3
CM30	71	1.28	5.8	6.4	80.9	323.7	11.9

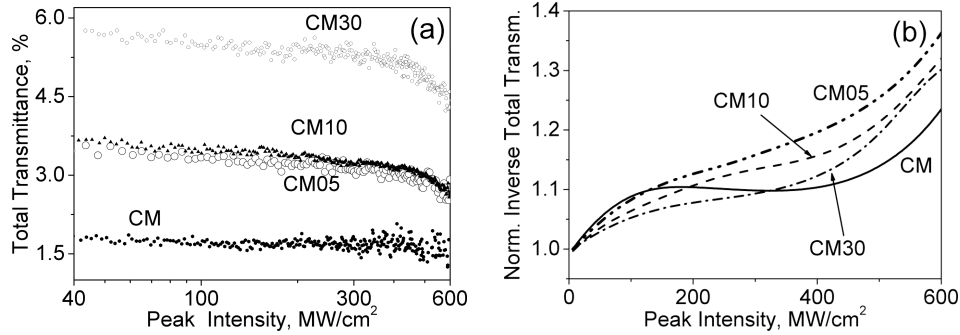


**Fig. 3.** Photoinduced variations of the total transmittance due to the self-action of picosecond laser pulses at 1064 nm: the absolute magnitude of total transmittance versus the peak laser intensity  $T(I)$  presented on semilogarithmic scale, each of the presented points corresponds to the averaged data collected over 25 laser shots (a); the smoothed inverse total transmittance data  $(T(I)/T_0)^{-1}$ , where  $T_0$  – the transmittance in a linear response regime (see Table 2) for the initial CM and the oxidized CMs (b)

the generation of functional groups, such as Cb and Ph, on the surface.

Figure 3, a shows that the oxidation of the CM results in an increase of the total transmittance, which is much more pronounced, when a porosity ( $p$ ) is reduced (see Table 2 for numerical data). We have attributed the transmittance  $T_0$  at the initial intensity range  $I < 2$  MW/cm<sup>2</sup> to a linear regime that decreases with an increase of  $I$ . In order to subtract a manifestation of the photoinduced effects from the linear response of a background, we normalized  $T(I)$  onto a linear transmittance,  $T_0$  (see Table 2). It is known that a characteristic feature of the two-photon absorption manifestation is the linear dependence of the inverse total transmittance on the laser intensity,  $(T(I)/T_0)^{-1} = 1 + \beta_{\text{eff}} L_{\text{eff}} I$ , in the plane wave approximation. The analysis of the averaged experimental data (see Fig. 3, b) has shown ranges with approximately permanent slopes at definite laser excitation levels. The first one (i) is observed for  $I < 90$  MW/cm<sup>2</sup>, where the efficient photodarkening up to  $\sim 6$ –10% of the CM samples was registered. The second one (ii) corresponds to the photodarkening saturation. The third (iii) one – to the following growth of the efficient inverse transmittance for  $400 < I < 600$  MW/cm<sup>2</sup>. The further  $I$  rise causes the CM porous layer ablation.

The calculated  $n_{\text{eff}}$  and the linear transmittances  $T_0$  for the studied samples are given in Table 2. Their magnitudes increase with a reduction in the porosity and agree with the results reported in [31, 37]. Consequently, the  $T_{\text{eff}}$  (Eq. (4)),  $\alpha_{\text{eff}}$  (Eq. (4)),

$\alpha_C$  (Eq. (7)), and the ratio of the  $\alpha_C$  to the  $S_{\text{BET}}$  were estimated. It was shown that the ratio  $\alpha_C/\alpha_{\text{eff}} \sim \sim 4.5$  that indicates that the optical absorption of carbon particles is significantly higher than that of their porous layer. The oxidation treatment results in a reduction of  $\alpha_C$  by about 1.9 times, which is accompanied by a decrease in the porosity by  $\sim 5\%$ . The effect of the oxidation on  $S_{\text{BET}}$  and the optical absorption at 1064 nm reveals the similar ratio of  $\alpha_C (S_{\text{BET}})^{-1} \sim 7.0 \times 10^{-2}$  kg/m<sup>3</sup> for the initial CM and slightly oxidized CM05 samples. For the samples treated with the concentrated HNO<sub>3</sub> (CM10 and CM30), the specific surface decreases faster than the optical absorption. This fact can be considered as a strong evidence of the optical absorption bulk response versus the interface contribution.

The photoinduced absorption occurs efficiently only at the so-called efficient self-action length  $L_{\text{eff}} < < d$  that is in a range 86.4–115.7  $\mu\text{m}$  for the studied CMs samples and is shorter than the porous layer thickness. About the 40-% reduction of the relative photoinduced transmittance variation  $\Delta T/T_0$  against the three-time rise of the linear transmittance  $T_0$  in CM30 versus the initial CM sample was observed.

From the experimental data presented in Fig. 3, b, the NLO absorption coefficients  $\beta_{\text{eff}}$  and  $\text{Im}(\chi_{\text{eff}}^{(3)})$  in range (i) were estimated according to the approach described in [27]. While  $\beta_{\text{eff}}/\text{Im}(\chi_{\text{eff}}^{(3)})$  reduces in the limits 3.0/2.5 for the sample CM30 versus the initial CM porous layer, the reduction of  $\beta_C/\text{Im}(\chi_C^{(3)})$  is more pronounced ( $\sim 3.5/4.0$ ) for the NLO response

**Table 3. NLO parameters of CMs versus the oxidation impact: the nonlinear absorption coefficients  $\beta_{\text{eff}}/\beta_C$  and imaginary parts of the cubic NLO susceptibility  $\chi_{\text{eff}}^{(3)}/\chi_C^{(3)}$  for the CM porous layers and their carbon particles fraction, correspondingly**

Sample	Carbon porous layer		Carbon particles fraction			
	$\beta_{\text{eff}}, \times 10^{-8} \text{ m/W}$	$\text{Im}(\chi_{\text{eff}}^{(3)}), \times 10^{-17} \text{ m}^2/\text{W}$	$\beta_C, \times 10^{-8} \text{ m/W}$	$\text{Im}(\chi_C^{(3)}), \times 10^{-16} \text{ m}^2/\text{W}$	$\beta_C/\alpha_C, \times 10^{-7}, \text{ m}^2/\text{W}$	$\frac{\text{Im}(\chi_C^{(3)})}{S_{\text{BET}}}$ *
CM	0.35	2.63	1.89	0.85	3.1	8.9
CM05	0.25	1.85	1.22	0.58	2.6	9.3
CM10	0.19	1.35	0.86	0.39	2.0	8.4
CM30	0.12	1.00	0.48	0.21	1.5	7.9

\*The values are represented without the power factor correction.

of the fraction of corresponding carbon particles. For higher CM oxidation levels (the CM samples treated with 10 and 30 mass%  $\text{HNO}_3$ ), the analysis of the rate of photoinduced absorption decrease in the linear response regime reveals a drastic decrease of the  $\beta_C/\alpha_C$  ratio.

The most promising result in the studied CMs was obtained for the variations of the  $\text{Im}(\chi_C^{(3)})/S_{\text{BET}}$  ratio that is close to the constant value of 8.6 within the experimental error range (does not exceed 20%) for the various levels of oxidation. The fact indicates the existence of a certain relation between the absorptive NLO response and the CM specific surface and supports the suggestion that the photoinduced variations of the absorption coefficient at a wavelength of 1064 nm (quantum energy of 1.17 eV) are related to the CM surface states.

For the given excitation wavelength, we have compared the efficiency of the registered NLO response due to the self-action of highly precise ps laser pulses with that for carbon nanoparticles (NPs) reported in the literature [16, 19, 38–40]. We accounted for the contribution of the carbon volume fraction ( $f_C$ ) in diluted NP colloid solutions, e.g., in toluene and chloroform [16], water [38], and N,N-dimethylformamide [19, 40], to the macroscopic NLO response within the EMA approach. For the binary system, within the approximation of a nonlinear splitting [41] and the negligible contribution of the solvent in its transparency range ( $\chi_{\text{sol}}^{(3)} = 0$ ), the NLO response of the composite can be given as:

$$\chi_{\text{eff}}^{(3)} = \frac{\chi_C^{(3)}}{f_C} \frac{\partial \varepsilon_{\text{eff}}}{\partial \varepsilon_C} \left| \frac{\partial \varepsilon_{\text{eff}}}{\partial \varepsilon_C} \right|. \quad (8)$$

For the  $\partial \varepsilon_{\text{eff}}/\partial \varepsilon_C$  expression within the Maxwell–Garnett averaging for diluted solutions, see [41]. The estimated  $\text{Im}(\chi_C^{(3)})$  magnitudes are  $\sim 0.34 \times 10^{-16}$  and  $\sim 1.3 \times 10^{-16} \text{ m}^2/\text{W}$  for  $\text{C}_{60}$ -fullerene and carbon dots [16], correspondingly. The close value of  $\sim 1.2 \times 10^{-16} \text{ m}^2/\text{W}$  is found for nanoscaled diamonds [40]. The values of  $\text{Im}(\chi_C^{(3)})$  enhance to  $\sim 8.4 \times 10^{-16}$  [38] and  $\sim 17 \times 10^{-16} \text{ m}^2/\text{W}$  [19] for a single and a few layered graphene oxides, correspondingly, under the excitation by ns laser pulses.

The comparison of the reference data with the experimentally obtained results has shown that the photoinduced absorption efficiency of bulk carbon particles,  $\text{Im}(\chi_C^{(3)}) \sim (0.21 \div 0.85) \times 10^{-16} \text{ m}^2/\text{W}$ , is in the range of the carbons NPs absorptive NLO response. The fact can reflect the same origin of the NLO response mechanism for the different carbon materials, including the nano-sized ones.

#### 4. Conclusion

Summarizing the findings, we can conclude that, for the first time, a contactless express method, which is based on the self-action of the picosecond laser pulses at 1064 nm, is used for the characterization of an optically dense porous layer of CM bulk particles. We report on the effect of the oxidation of carbons on their photoinduced total transmission and related opto-mechanical parameters as the quality of carbon media subjected to the oxidation, which is the initial step of the most commonly used functionalization routes for the preparation of biomedical materials. It is shown that the linear optical absorption and the nonlinear optical response are sensitive to the oxidation intensity of the initial CM.

On the example of carbons obtained from a ligno-cellulosic source, it is found that the oxidation caused a reduction of the  $S_{\text{BET}}$  surface area from  $9.52 \times 10^5$  to  $2.73 \times 10^5$   $\text{m}^2/\text{kg}$ . It is realized due to the destruction of a part of the carbon matrix and to the formation of novel O-containing surface groups. The surface functional groups are determined in a dynamic argon atmosphere by the thermogravimetric (TG) analysis and thermo-programmed desorption coupled with IR (TPD-IR) spectroscopy. The surface acidity defined from data of the Boehm titration shows the acceptable agreement with the data of the TG-TPD-IR examination. We have revealed that the CM surface becomes less hydrophobic after the oxidative treatment by  $\text{HNO}_3$  due to the presence of the functional groups. The concentrated 30-mass%  $\text{HNO}_3$  is found to be the most efficient oxidant that gives the highest yield of Cb, A-L, and Ph surface functionalities. The oxidation decreases the porosity by  $\sim 7\%$  and reduces the values of optical absorption of the fraction of carbon particles  $\alpha_c$  by about 1.9 times, while the specific surface  $S_{\text{BET}}$  decreases faster than the  $\alpha_c$ . This fact can be considered as a strong evidence of the linear optical absorption bulk response versus the interface contribution.

The analysis of the rate of decrease of the nonlinear absorption coefficient in the linear response regime shows the drastic decrease of the  $\beta_c/\alpha_c$  ratio for a higher CM oxidation level. It is worth to outline a slight variation of the ratio  $\text{Im}(\chi_C^{(3)})/S_{\text{BET}}$  (the deviation does not exceed 20%) within the more than three-time oxidation-induced reduction in  $S_{\text{BET}}$ . It indicates a certain correlation between the absorptive NLO response and the CM specific surface.

We have experimentally proved that the photoinduced absorption efficiency of the bulk carbon particles  $\text{Im}(\chi_C^{(3)}) \sim (0.21 \div 0.85) \times 10^{-16}$   $\text{m}^2/\text{W}$  is in the range of that for nano-sized carbons. This fact can reflect the same origin of the nonlinear response mechanism for different carbon materials, including NPs. The enhancing of the surface hydrophilicity allows the use of a carbon matrix for the covalent binding of bioligands, amino acids, their residues, and proteins to the oxygen-containing functionalities such as Cb groups. The further improvement of the adhesion characteristics may be achieved by varying different oxidation techniques under a control with the pulsed laser radiation self-action response read-out technique.

The authors V.Ya.G., A.V.U., and V.V.M. acknowledge a partial support by grant V-166 of the NAS of Ukraine. One of the authors, V.V.L., acknowledges a partial financial support from the National Scholarship Program of the Slovak Republic for the Mobility of Students, Ph.D. Students, University Teachers, Researchers and Artists, SAIA Grant, n.o., and the Agency of Ministry of Education, Science, Research, and Sport of the Slovak Republic, the project ITMS: 26110230119.

1. R.J. Hunter and V.R. Preedy, *Nanomedicine in Health and Disease* (CRC, Boca Raton, 2012).
2. M.J. Schulz and V.N. Shanov, *Nanomedicine Design of Particles, Sensors, Motors, Implants, Robots, and Devices* (Artech House, Boston-Norwood, 2009).
3. Z. Li, S. Wu, Z. Zhao, and L. Xu, Influence of surface properties on the interfacial adhesion in carbon fiber/epoxy composites, *Surf. Interface Anal.* **46**, 16 (2014) [DOI: 10.1002/sia.5340].
4. S.F. Waseem, S.D. Gardner, G. He et al., Adhesion and surface analysis of carbon fibres electrochemically oxidized in aqueous potassium nitrate, *J. Mater. Sci.* **33**, 3151 (1998) [DOI: 10.1023/A:1004304124799].
5. T.J. Webster, M.C. Waid, J.L. McKenzie, R.L. Price, and J.U. Ejiogor, Nano-biotechnology: carbon nanofibres as improved neural and orthopaedic implants, *Nanotechnology* **15**, 48 (2004) [DOI: 10.1088/0957-4484/15/1/009].
6. M. Yang, Y. Liang, Q. Gui, J. Chen, and Y. Liu, Electroactive biocompatible materials for nerve cell stimulation, *Mater. Res. Express* **2**, 042001 (2015) [DOI: 10.1088/2053-1591/2/4/042001].
7. C.S.S.R. Kumar, *Nanomaterials for Biosensors* (Wiley, Weinheim, 2007).
8. P. Morgan, *Carbon Fibers and Their Composites* (CRC, Boca Raton, 2005).
9. L.-G. Tang, and J.L. Kardos, A review of methods for improving the interfacial adhesion between carbon fiber and polymer matrix, *Polym. Compos.* **18**, 100 (1997) [DOI: 10.1002/pc.10265].
10. P.W. Yip and S.S. Lin, Effect of surface oxygen on adhesion of carbon fiber reinforced composites, *MRS Proc.* **170**, 339 (1989) [DOI: 10.1557/PROC-170-339].
11. R.L. Price, K.M. Haberstroh, and T.J. Webster, Improved osteoblast viability in the presence of smaller nanometre dimensioned carbonfibres, *Nanotechnology* **15**, 892 (2004) [DOI: 10.1088/0957-4484/15/8/004].
12. D.J. Hak, C. Mauffrey, D. Seligson, and B. Lindeque, Use of carbon-fiber-reinforced composite implants in orthopedic surgery, *Orthopedics* **37**, 825 (2014) [DOI: 10.3928/01477447-20141124-05].
13. R. Hillock and S. Howard, Utility of carbon fiber implants in orthopedic surgery: literature review, *JISRF Recon. Rev.* **4**, 23 (2014) [DOI: 10.15438/rr.v4i1.55].

14. C.S. Li, C. Vannabouathong, S. Sprague, and M. Bhandari, The use of carbon-fiber-reinforced (CFR) PEEK material in orthopedic implants: A systematic review, *Clin. Med. Insights Arthritis Musculoskelet Disord.* **8**, 33 (2015) [DOI: 10.4137/CMAMD.S20354].
15. S.C. Tjong *Advances in Biomedical Sciences and Engineering*, edited by S.C. Tjong (Bentham, Hong-Kong, 2009), p. 143.
16. P. Aloukos, I. Papagiannouli, A.B. Bourlinos *et al.*, Third-order nonlinear optical response and optical limiting of colloidal carbon dots, *Optics Exp.* **22**, 12013 (2014) [DOI: 10.1364/OE.22.012013].
17. A.B. Bourlinos G. Trivizas, M.A. Karakassides *et al.*, Green and simple route toward boron doped carbon dots with significantly enhanced non-linear optical properties, *Carbon* **83**, 173 (2015) [DOI: 10.1016/j.carbon.2014.11.032].
18. I.M. Belousova D.A. Videnichev, I.M. Kislyakov *et al.*, Comparative studies of optical limiting in fullerene and shungite nanocarbon aqueous dispersions, *Opt. Mater. Exp.* **5**, 169 (2015) [DOI: 10.1364/OME.5.000169].
19. S. Couris and N. Liaros, *Proc. of 16th Intern. Confer. on Transparent Optical Networks (ICTON)*, edited by M. Jaworski, and M. Marciniak (IEEE & National Institute of Telecommunications, Warsaw, 2014), p. 1 [DOI: 10.1109/ICTON.2014.6876558].
20. M.G. Papadopoulos, A.J. Sadlej, and J. Leszczynski, *Non-Linear Optical Properties of Matter: From Molecules to Condensed Phases* (Springer, Dordrecht, 2006).
21. V.E. Diyuk, A.N. Zaderko, K.I. Veselovska, and V.V. Lisnyak, Functionalization of surface of carbon materials with bromine vapors at mediate high temperature: a thermogravimetric study, *J. Therm. Anal. Calorim.* **120**, 1665 (2015) [DOI: 10.1007/s10973-015-4495-2].
22. K.-C. Xie, *Structure and Reactivity of Coal* (Springer, Berlin, 2015).
23. S.L. Goertzen, K.D. Thériault, A.M. Oickle *et al.*, Standardization of the Boehm titration. Part I. CO<sub>2</sub> expulsion and endpoint determination, *Carbon* **48**, 1252 (2010) [DOI: 10.1016/j.carbon.2009.11.050].
24. A.M. Oickle, S.L. Goertzen, K.R. Hopper *et al.*, Standardization of the Boehm titration: Part II. Method of agitation, effect of filtering and dilute titrant, *Carbon* **48**, 3313 (2010) [DOI: 10.1016/j.carbon.2010.05.004].
25. V.E. Diyuk, A.N. Zaderko, L.M. Grishchenko *et al.*, Efficient carbon-based acid catalysts for the propan-2-ol dehydration, *Catal. Commun.* **27**, 33 (2012) [DOI: 10.1016/j.catcom.2012.06.018].
26. K.I. Veselov'ska, V.L. Veselov'skyi, O.M. Zaderko *et al.*, Effect of the oxidation and thermal treatment on bromination of activated carbon, *J. Superhard Mater.* **37**, 39 (2015) [DOI: 10.3103/S1063457615010062].
27. V.Ya. Gayvoronsky, A.S. Popov, M.S. Brodyn *et al.*, in: *Nanocomposites, Nanophotonics, Nanobiotechnology, and Applications*, edited by O. Fesenko, and L. Yatsenko (Springer, Heidelberg, 2015).
28. W.L. Smith, in: *CRC Handbook of Laser Science and Technology*, edited by M.J. Weber (CRC, Boca Raton, 1988).
29. H. Looyenga, Dielectric constants of heterogeneous mixtures, *Physica* **31**, 401 (1965) [DOI: 10.1016/0031-8914(65)90045-5].
30. S.O. Nelson, D.P. Lindroth, and R.L. Blake, Restricted access. Dielectric properties of selected minerals at 1 to 22 GHz, *Geophysics* **54**, 1344 (1989) [DOI: 10.1190/1.1442596].
31. J.G. Speight, *The Chemistry and Technology of Coal* (CRC, Boca Raton, 2012).
32. J.L. Figueiredo, M.F.R. Pereira, M.M.A. Freitas, and J.J.M. Orfão, Modification of the surface chemistry of activated carbons, *Carbon* **37**, 1379 (1999) [DOI: 10.1016/S0008-6223(98)00333-9].
33. W. Shen, Z. Li, and Y. Liu, Surface chemical functional groups modification of porous carbon, *Rec. Pat. Chem. Eng.* **1**, 27 (2008) [DOI: 10.2174/2211334710801010027].
34. V.E. Diyuk, R.T. Mariychuk, and V.V. Lisnyak, Barothermal preparation and characterization of micro-mesoporous activated carbons, *J. Therm. Anal. Calorim.* **124**, 1119 (2016) [DOI: 10.1007/s10973-015-5208-6].
35. L.P. Vera, J.A. Pérez, and H. Riascos, Spectroscopic study of emission coal mineral plasma produced by laser ablation, *J. Phys.: Conf. Ser.* **511**, 012063 (2014) [DOI: 10.1088/1742-6596/511/1/012063].
36. R. Zhang, Y. Achiba, K.J. Fisher *et al.*, Laser ablation mass spectrometry of pyrolyzed Koppers coal-tar pitch: a precursor for fullerenes and metallofullerenes, *J. Phys. Chem. B* **103**, 9450 (1999) [DOI: 10.1021/jp9910791].
37. B.J. Stagg and T.T. Charalampopoulos, Refractive indices of pyrolytic graphite, amorphous carbon, and flame soot in the temperature range 25° to 600 °C, *Combust. Flame* **94**, 381 (1993) [DOI: 10.1016/0010-2180(93)90121-I].
38. N. Liaros, P. Aloukos, A. Kolokithas-Ntoukas *et al.*, Non-linear optical properties and broadband optical power limiting action of graphene oxide colloids, *J. Phys. Chem.* **117**, 6842 (2013) [DOI: 10.1021/jp400559q].
39. S. Husaini, A. Lesko, E.M. Heckman, and R.G. Bedford, Engineered bio-compatible graphene nanomaterials for nonlinear applications, *Opt. Mater. Exp.* **5**, 102 (2015) [DOI: 10.1364/OME.5.000102].
40. I. Papagiannouli, A.B. Bourlinos A. Bakandritsos, and S. Couris, Nonlinear optical properties of colloidal carbon nanoparticles: nanodiamonds and carbon dots, *RSC Adv.* **4**, 40152 (2014) [DOI: 10.1039/C4RA04714A].
41. E.F. Venger, A.V. Goncharenko, and N.L. Dmitruk, *Optics of Small Particles and Dispersed Media* (Naukova Dumka, Kyiv, 1999) (in Ukrainian).

Received 05.04.16

А.В. Уклеїн, В.Є. Діюк,  
Л.М. Грищенко, В.О. Кожанов, В.В. Лісняк,  
В.В. Мультиян, П.І. Будник, В.Я. Гайворонський

#### КОРЕЛЯЦІЯ МІЖ ФОТОІНДУКОВАНИМ ПОВНИМ ПРОПУСКАННЯМ ТА СТУПЕНЕМ ФУНКЦІОНАЛІЗАЦІЇ ПОВЕРХНІ ВУГЛЕЦЕВИХ МАТЕРІАЛІВ, ОДЕРЖАНИХ З ПРИРОДНИХ ПОНОВЛЮВАНИХ ДЖЕРЕЛ

#### Резюме

Вперше було застосовано швидкий безконтактний метод, який базується на самовпливі пікосекундного лазерного випромінювання на довжині хвилі 1064 нм, для характеристики оптично густих пористих шарів об'ємних частинок карбонових матеріалів (КМ), що отримані з лігноцелюлозної сировини. Показано, що окислювальна обробка призводить до зменшення площі поверхні Брунауера–Еммета–Тейлора ( $S_{\text{ВЕТ}}$ ) від  $9,52 \cdot 10^5 \text{ м}^2/\text{кг}$  до  $2,73 \cdot 10^5 \text{ м}^2/\text{кг}$ , яка відбувається за рахунок руйнування частини вуглецевої матриці та формування нових О-вмістних поверхневих груп. Найбільш ефективним окиснювачем виявлено концентровану  $\text{HNO}_3$  30 мас.%, яка приводить до найефективнішого утворення

карбоксильних, ангідридних і лактонних, та фенольних поверхневих груп. Концентрацію таких функціональних груп було визначено в динамічній атмосфері аргону за допомогою термогравіметричного аналізу (ТГ) і термопрограмованої десорбції, що поєднується із ІЧ (ТПД–ІЧ) спектроскопією. Кислотність поверхні, яка визначалася за даними титрування за Бьомом, добре узгоджується із даними ТГ–ТПД–ІЧ досліджень. Підвищення гідрофільності поверхні дозволяє застосовувати вуглецеву матрицю для ковалентного зв'язування біолігандів, амінокислот, їх похідних і протеїнів з кисневмісними функціональними карбоксильними групами. Отримані значення ефективності фотоіндукованого поглинання  $\text{Im}(\chi_C^{(3)}) \sim 10^{-16} \text{ м}^2/\text{В}$  добре збігаються з відповідними для нанорозмірних КМ. Показано, що відношення  $\text{Im}(\chi_C^{(3)})/S_{\text{ВЕТ}}$  є майже сталим у межах експериментальної похибки. Це вказує на певну кореляцію між абсорбційним нелінійно-оптичним відгуком та питомою поверхнею КМ. Ми пропонуємо використати  $\text{Im}(\chi_C^{(3)})$  як параметр якості карбонових матеріалів в процесі їх окиснення. Окиснення є типовим початковим кроком найпоширеніших методів функціоналізації КМ для біомедицинських застосувань.